Science of the Total Environment 732 (2020) 139249

Contents lists available at ScienceDirect

Science of the Total Environment

journal homepage: www.elsevier.com/locate/scitotenv

The effects of long-term saline groundwater pumping for desalination on the fresh–saline water interface: Field observations and numerical modeling

Shaked Stein [a,b,c,**], Fernando Sola [d], Yoseph Yechieli [b,c], Eyal Shalev [b], Orit Sivan [a], Roni Kasher [c], Angela Vallejos [d,*]

[a] Department of Geological and Environmental Sciences, Ben-Gurion University of the Negev, Beer Sheva 84105, Israel
[b] Geological Survey of Israel, 32 Yesha'ayahu Leibowitz, Jerusalem 9692100, Israel
[c] Zuckerberg Institute for Water Research, Jacob Blaustein Institutes for Desert Research, Ben-Gurion University of the Negev, Sde Boqer Campus, Midreshet Ben-Gurion 84990, Israel
[d] Water Resources and Environmental Geology, University of Almería, Almería 04120, Spain.

HIGHLIGHTS

- Desalination plant operates on Almeria's shore, feeding from saline groundwater.
- First field study on coastal aquifer response to pumping of saline groundwater.
- Numerical hydrological model was established and calibrated with the field data.
- Long-term interface monitoring shows seaward shift in its location.
- 3D model results show general freshening of the aquifer after 12 years of pumping.

GRAPHICAL ABSTRACT

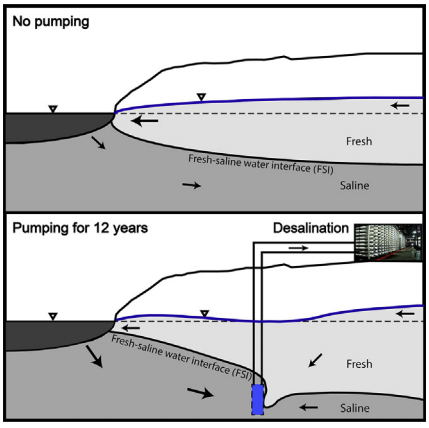

ARTICLE INFO

Article history:
Received 16 March 2020
Received in revised form 4 May 2020
Accepted 4 May 2020
Available online 11 May 2020

Editor: José Virgílio Cruz

Keywords:
Seawater intrusion
Desalination
Saline groundwater

ABSTRACT

This study tests for the first time the long-term effects of pumping saline groundwater (SGW) as feed for a desalination plant on a coastal aquifer. Field measurements combined with 3D modeling of the hydrological conditions were conducted to examine the effects of SGW pumping on the aquifer system. The plant is next to the city of Almeria (South East Spain) and has been operating since 2006. It uses multiple beach wells along the shore to draw SGW from beneath the fresh–saline water interface (FSI) of the Andarax coastal aquifer. The long-term impact of the intensive pumping on the aquifer was assessed by electrical conductivity profiles in three observation wells during 12 years of pumping. The FSI deepened with continuous pumping, reaching a decrease of ~50 m in the observation well closest to the pumping wells. A calibrated three-dimensional numerical model of the Andarax aquifer replicates the freshening of the aquifer due to the continuous pumping, resulting in a salinity decrease of ~16% in the vicinity of the wells. The salinity decrease stabilizes at 17%, and the model predicts no further significant decrease in salinity for additional 20 years. Submarine groundwater discharge is

* Corresponding author.
** Correspondence to: S. Stein, Department of Geological and Environmental Sciences, Ben-Gurion University of the Negev, Beer Sheva 84105, Israel.
E-mail addresses: shakedst@post.bgu.ac.il (S. Stein), avallejo@ual.es (A. Vallejos).

https://doi.org/10.1016/j.scitotenv.2020.139249

Coastal aquifer management

lowered due to the SGW pumping and ~19,000,000 m^3 of freshwater has not lost to the sea during the 12 years of pumping with a rate of ~1,100,000 m^3 yr^{-1} after 6 years of pumping. After pumping cessation, hydrostatic equilibrium would take about 20 years to recover. This work presents the complex dynamics of the FSI due to the SGW pumping for desalination in the first real long-term scenario. It shows by combining field work and numerical modeling, a significant freshening of the aquifer by pumping SGW, emphasizing an additional advantage and the effectiveness of this use as a negative hydraulic barrier against seawater intrusion.

1. Introduction

The transition zone between fresh and saline groundwater (SGW) in coastal aquifers has been extensively studied. Many authors have examined the development of the fresh–saline water interface (FSI) and regional flow regimes (Bear, 1979; Cooper, 1959; Kohout, 1960; Todd and Mays, 1980), and the physical processes affecting the depth and thickness of the FSI due to natural causes such as tides, storms, and rising sea level (Ataie-Ashtiani et al., 1999; Bear, 1972; Van Dam, 1999; Levanon et al., 2017; Loáiciga et al., 2012; Michael et al., 2005; Strack, 1976; Wang and Tsay, 2001; Werner and Simmons, 2009; Yechieli et al., 2010).

Natural groundwater flow is affected by human activities e.g., pumping (Houben and Post, 2017; Zhou et al., 2005). The conoid of piezometric depression produced by the pumping of freshwater forms a dome of higher-salinity water beneath it (upconing) to compensate the deficit in the hydrostatic weight generated by pumping (Jakovovic et al., 2016; Werner et al., 2009). As a result, abstraction enhances the intrusion of seawater into the aquifer (Houben and Post, 2017; Werner et al., 2013), leading to loss of freshwater through salinization of the surrounding aquifer, in some cases tens of kilometers away (Knight et al., 2018; Yu and Michael, 2019). The addition of only 5% seawater to freshwater makes it no longer potable or suitable for agriculture (Custodio and Bruggeman, 1987). Thus, seawater intrusion and the salinization of coastal aquifers constitute an important environmental problem worldwide (Ferguson and Gleeson, 2012; Kazakis et al., 2018; Werner et al., 2012). This concern is especially severe given current worldwide water shortages, which have increased significantly owing to population growth and climate change.

Negative hydraulic barriers, formed by pumping seawater from a coastal aquifer lower the saltwater head and can mitigate seawater intrusion, thus limiting the intrusion of salt water into the aquifer and allowing freshwater to accumulate beyond the barrier (Dhar and Datta, 2009; Sreekanth and Datta, 2011; Todd and Mays, 1980). However, beach wells established for this purpose also extract some freshwater from the aquifer system over time (Otero et al., 2011; Pool and Carrera, 2009; Stein et al., 2019). The impact of pumping seawater from the aquifer on the geometry of the FSI is not as clear as in the case of pumping freshwater. Pumping freshwater and its implication on the coastal hydrology has drawn great attention from groundwater experts however the movement of the FSI due to pumping of SGW was neglected. Given the high salinity and generally low economic value of SGW, the literature describes few examples of its large-scale saline water pumping from a coastal aquifer. Reported examples are mostly related to supplying desalination plants (Daniele et al., 2011; Ghaffour et al., 2015; Jorreto et al., 2009; Otero et al., 2011; Ros and Zuurbier, 2017; Sola et al., 2014; Stein et al., 2016, 2019) as well as pumping for fish farms (Nocchi and Salleolini, 2013).

The use of SGW as a feed source for desalination entails less maintenance and consumes less energy than the use of seawater, making it economically attractive (Dehwah and Missimer, 2016; Ghaffour et al., 2013; Missimer et al., 2013; Sola et al., 2013; Stein et al., 2016). Additionally, SGW possesses more stable temperature than seawater, undergo natural filtration through the porous medium and result in less fouling on the reverse osmosis membrane (Sola et al., 2013; Stein et al., 2016). Consequently, in recent years, desalination plants increasingly use subsurface seawater as their feed stream (Missimer et al., 2013; Pulido-Bosch et al., 2019; Rachman et al., 2014; Rodríguez-Estrella and Pulido-Bosch, 2009). Long-term field data for large scale pumping of SGW are required to provide a better understanding of the hydrological system and verify hydrological models.

The present work quantifies the response of the FSI over several years of SGW pumping (to feed a desalination plant) as well as the long and short-term variations in response to stopping pumping, by combining field data with numerical modeling. This is done by using continuous monitoring of water electrical conductivity (EC) over 12 years in three observation wells located near the wells that pump the SGW, and also by groundwater flow and transport modeling that simulates the response of the aquifer to the pumping. The results show the effects of pumping SGW for a desalination plant on groundwater flow and salinity, and its effectiveness as a negative hydraulic barrier against seawater intrusion.

2. Hydrogeological setting

The Andarax Delta is situated on the Mediterranean coast of SE Spain (Fig. 1). A detrital aquifer runs along the entire length of the Andarax River valley. It includes Quaternary materials, both alluvial and deltaic, together with Pliocene deltaic sandy silt conglomerates (Sanchez-Martos et al., 2002). Aquifer materials in the delta correspond to deltaic formations with a clear marine influence, in lateral continuity with the alluvial materials. The bottom of the aquifer comprises Pliocene silts with interbedded sands, calcarenites, and conglomerates (Aguirre et al., 1996). The region has a semiarid climate with average rainfall not exceeding 200 mm yr^{-1} (Pulido-Bosch et al., 2012). The Andarax River basin (total area 2100 km^2) has been strongly modified by human activities. Water intake from the river for irrigation means that no water reaches the river mouth throughout most of the year, except during floods which occur once or twice a year.

The study site is located on the Andarax River delta, where a plant desalinates SGW. Water is pumped from 19 beach wells with 18″ diameter, ranging in depth from 78 to 154 m and screened for the last 20 to 40 m. The wells are distributed along the southern part of the delta, parallel to the coastline and 30–150 m from the sea (Fig. 1). Three additional observation wells (P—I, P-II, and P-III) are located along the coast following the main direction of groundwater flow. Their perpendicular distances to the coast are 130, 150, and 260 m, respectively (Figs. 1 and 2). They were designed to monitor the spatial and temporal hydrodynamic evolution of the FSI. Table 1 lists observation well distances from the shore and data on well perforation. The pumping and observation wells intersect the aquifer material, which reaches a total depth of about 100 m. The average transmissivity of the aquifer materials is 6500 m^2 d^{-1} (Sánchez-Martos et al., 2007).

3. Methodology

3.1. Electrical conductivity logs

Measurements of electrical conductivity (EC) and water temperature commenced in the three observation wells in 2005, before the desalination plant started pumping in November 2006. No data were collected between 2008 and 2016. Continuous pumping since the

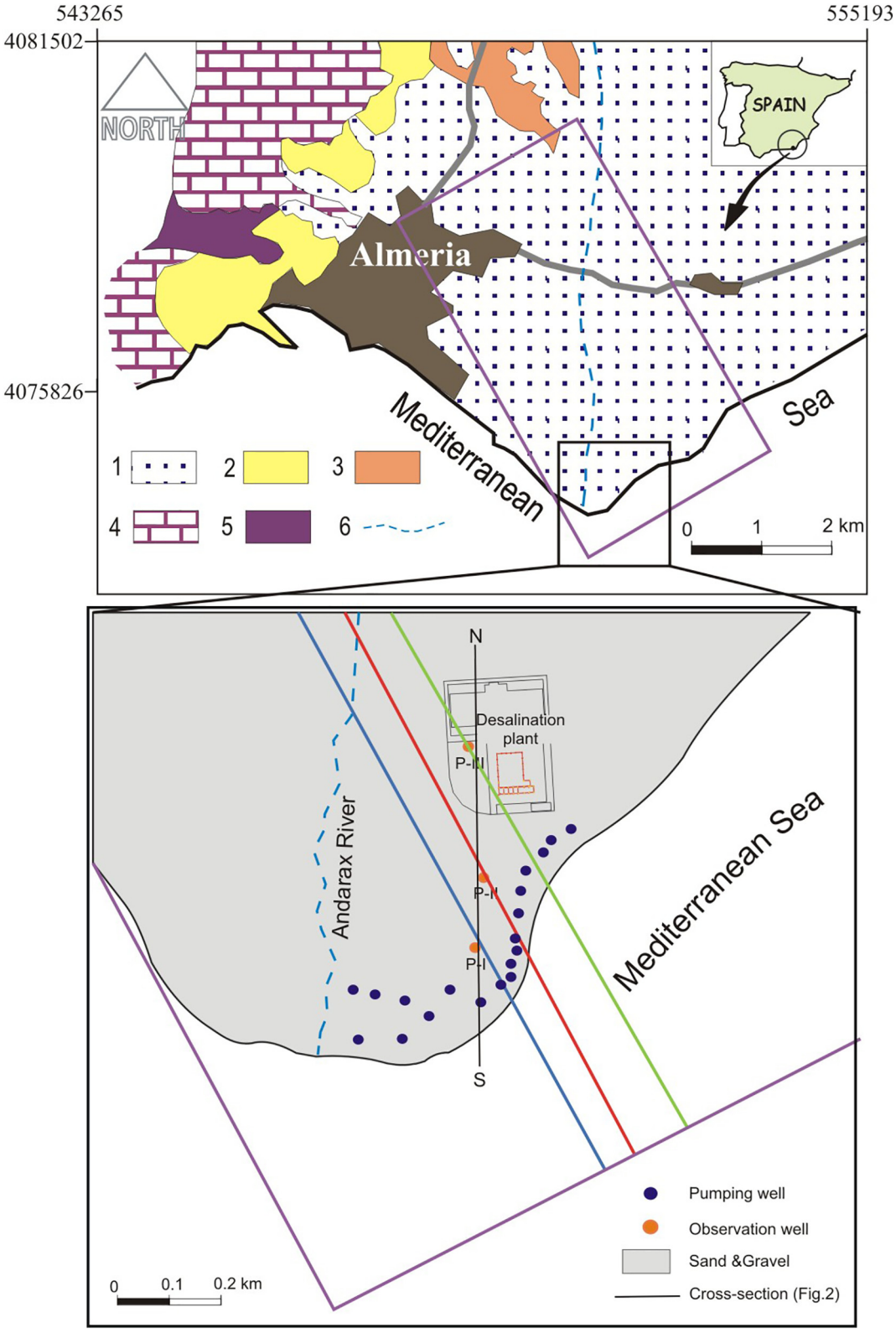

Fig. 1. Location of the study area and its geological context (1: sand and gravel, 2: silt and sand, 3: calcarenite, 4: dolostone, 5: phyllite). Purple rectangle represents the 3D model domain. The blue, red, and green lines indicate the locations of cross-sections (shown in Fig. 6) crossing the observation wells.

plant went into operation has enabled long-term monitoring of the aquifer under the influence of this regime (2006–2018) and comparison with data collected before pumping. No measurements were obtained from 2008 to 2016, therefore, three years of data collection is presented. The EC logs were conducted using down-hole logging equipment (GeoVista), which measures temperature and EC every 10 cm throughout the well, and also using a multi-meter probe (Solinst 107 TLC meter). It is important to mention that long screened wells provide high error regarding hydraulic conductivity measurements and bias the results (Rau et al., 2019). Furthermore, long screens in wells disrupt

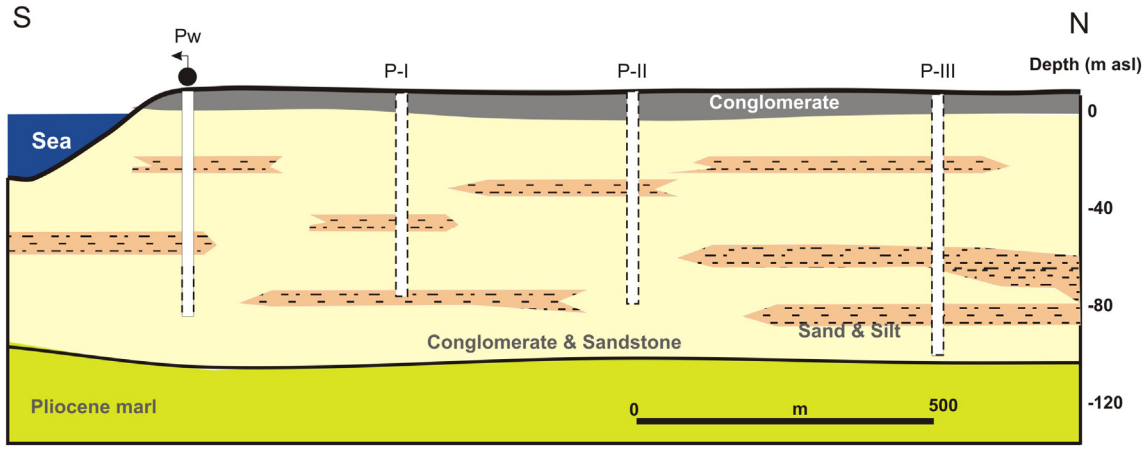

Fig. 2. Schematic cross-section of the Andarax aquifer including the pumping wells (Pw) and observation wells P-I, P-II, and P-III, and their distances from shore. The perforated sections of the wells are indicated by dash lines.

Table 1
Basic information on groundwater observation wells used in this study.

Observation well	Diameter	Distance from shore [m]	Drilling depth [m]	Ground elevation [m asl][a]	Bottom elevation [m asl]
P-I	6.5"	120	78	2.1	−75.9
P-II	6.5"	150	82	4.9	−77.1
P-III	6.5"	260	100	4.9	−95.1

[a] m asl: meters above sea level.

the natural vertical density stratification and may not represent the real situation in the aquifer. However, measurements of EC in these wells can provide information for studying the FSI dynamics. The operation regime of the plant consists of pumping (up to 4000 $m^3\ h^{-1}$) for 12 h overnight and shutting down during the day (due to lower night-time energy costs). Not all wells pump at the same time due to technical criteria, but the total volume is always the same. Logs were recorded 1–2 h after pumping had ceased on each occasion. Furthermore, over a 72 h cycle of no pumping, six vertical logs were measured to assess the effect of an extended break in pumping on the EC of the aquifer. These measurements were made during 7–10 December 2016.

The EC of seawater in this area of the Mediterranean Sea is about 60 mS cm^{-1}, comparable to that in the deepest and most saline parts of the aquifer. The geometry of the FSI is defined using a 50% seawater EC isoconcentration line (30 mS cm^{-1}).

3.2. Numerical model

A 3D model representing the coastal aquifer near the desalination plant was constructed (Fig. 3) to simulate aquifer hydrology as SGW is pumped to the plant. The model code used in this study was the numerical software FEFLOW (Diersch and Kolditz, 2002) that employs a finite element solution for the variable density flow coupled with solute transport processes. The model was constructed as 25 vertical layers with dimensions of 5.5 km long, 3 km wide, and 100 m deep. The mesh is triangular prismatic with 1,236,192 elements and 663,550 nodes (see supplementary information, Fig. S1). This is with homogeneous and anisotropic hydraulic properties, which is a simplification of the field site as described above. It is well known that salt water intrusion process is sensitive to confining layers and heterogeneity of the porous media. However, the model was simplified to prevent numerical error and long computational time. All pumping wells in the model are screened at 70–100 m below sea level, and are located 50 m from the shore, which is the average distance of the pumping wells in the field. The pumping wells are placed with two zones of well density as there are more pumping wells within the same radius from P-I as from P-II and P-III (Fig. 1). High density of wells is modeled next to P-I where lower pumping well density is present from both sides of this zone (Fig. 3). A pumping rate of 4000 $m^3\ h^{-1}$, corresponding to the set of daily operating wells and representative of 12 years of operation, was applied.

Fig. 3 shows the model boundary conditions (2D representation of the model and boundary conditions can be seen in Fig. S2). A seawater head boundary condition was applied on the sea; no-flow boundary conditions were applied on the bottom and sides of the model as the model is aligned with water flow direction; an inflow of freshwater was applied from the land side; and rain infiltration was applied at the top boundary. The salt concentration at the seawater boundary is 35 g L^{-1}. The infiltration of freshwater at the top boundary was set to 30 mm yr^{-1}, which is representative of the regional climate and a typical infiltration ratio of 0.15. The land-side boundary was set to a constant flow of 8.5 mm d^{-1}, as determined during the calibration process (see Section 4.2). The hydraulic parameters (hydraulic conductivity anisotropy, porosity, and dispersivity) were also determined during the calibration.

4. Results and discussion

4.1. Interface monitoring

4.1.1. Long-term interface monitoring

Monitoring of the FSI started one year prior to pumping start and continued for additional 1 year thereafter and for another year between October 2016 to February 2018. From this data, the steady-state FSI location was determined, and the FSI location change with time was recorded for the three observation wells (Fig. 4). Over 12 years of pumping, the FSI shifted downward. Its position is described using two isoconductivity lines (25% and 75%, derived from 100% seawater conductivity of 60 mS cm^{-1}) that contain the interface zone (Fig. 4). Groundwater with EC below 25% is considered fresh or brackish, and that with a value above 75% is saltwater.

In observation well P-I, located 120 m from the pumping well, the interface descended by 20 m within the first year of pumping at the desalination plant (starting November 2006), and continued to descend an additional 30 m by 2018. At P-II, the EC evolved similarly, but the interface descended by only 35 m after 12 years. Observation well P-III was the most stable due to its large distance from the pumping wells. There, the FSI dropped by 15 m after 12 years of pumping (Fig. 4c). These results are consistent with Jorreto et al. (2009), who reported a salinity decrease at this site after several months of pumping, using EC divers and electrical resistivity tomography analysis. The width of the

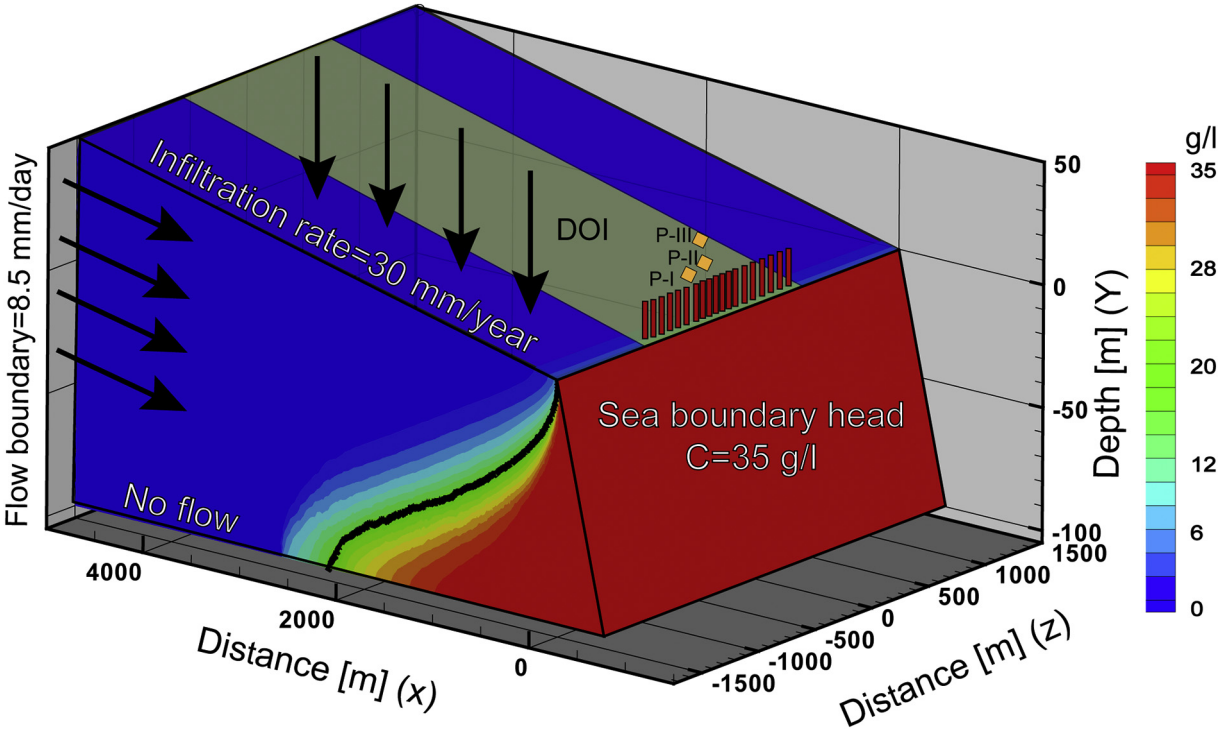

Fig. 3. The 3D model domain and boundary conditions at steady state. Black arrows represent inflows. No-flow boundaries are used on the sides and bottom. The black line represents the 50% salinity contour (FSI). Pumping wells are shown as red cylinders, and observation wells are marked by orange diamonds. The dark yellow box represents the domain of interest (DOI), which stretches under the land side and to the bottom of the aquifer.

interface in P-I and P-II seems to decrease after pumping start while in P-III, the width of the FSI remained relatively unchanged (Fig. 4). The desalination plant operator reported that the pumped water salinity after 12 years is ~33 g L^{-1}.

4.1.2. Short-term interface monitoring

The aquifer recovery (the FSI shift toward hydrostatic equilibrium) is examined over two different time scales: short-term daily (field data and model) and long-term over 20 years (model). In addition to their daily shut down, the pumps were stopped on one occasion for three full days in December 2016. At this time, EC profiles of the three observation wells were recorded immediately after the pumping stopped and again after 1, 5, 12, and 72 h (Fig. 5). During this event, the FSI shifted upward in all wells, denoting aquifer salinization and recovery toward its original location under natural steady state conditions. The return of the hydrological system to its natural state before pumping is dictated by the hydrostatic equilibrium between the fresh and saline groundwater.

The smallest change in EC was recorded at P-III both during pumping and after the pumping stopped. This was probably due to its location farthest from the pumping wells. The greatest change during recovery was recorded at P-II, which has the longest section of screen (82 m) among the three boreholes (Table 1). A long screen serves as a "short circuit" for water in the aquifer, as it forms a hydraulic connection between zones of different hydraulic head in the aquifer, thus biasing the results (Levanon et al., 2013; Shalev et al., 2009). The FSI changes observed in the field after three days of recovery were 12, 25, and 0 m at wells P-I, P-II, and P-III, respectively (Fig. 5). The model results, in contrast, were 0.9, 0.5, and 0.1 m, respectively (shown in details in Section 4.3). The "short circuit" phenomenon accounts for the difference between the two sets of results. This phenomenon is assumed to be local in scale, related to the long sections of screened wells and thus is not representative of the whole aquifer. Shalev et al. (2009) showed that in a mixing zone, model calculations can be up to one order of magnitude lower than field measurements from monitoring boreholes with long sections of screen. Our results appear to demonstrate this contrast. Although monitoring the FSI width and movement in long screened wells is not preferable, this data can provide important information about the FSI behavior and rates when pumping starts or stops.

4.2. Model calibration

Initial conditions were established by running the model without pumping. Hydraulic parameters were modified until a good fit was achieved between the FSI depth in the model and the data measured at the observation wells prior to pumping. Additional parameters calibrated with the model include the hydraulic conductivity anisotropy and the horizontal freshwater inflow. The porosity is assigned using previous pumping data while the FSI depth after 1 year of pumping was measured and compared to the data, as the FSI velocity is connected to the aquifer's porosity. Table 2 summarizes the hydraulic parameters used in the model that were determined by trial and error during the dual calibration process. Fig. 6 shows the modeled 50% salinity lines of each cross-section that intercepts the three observation wells. The colors in the figure correspond to the color lines in Fig. 1. The calibration precision is verified by the three modeled cross sections and their good fit to the data at steady state and with time after 1 year and 12 years of pumping.

4.3. Modeling aquifer response to saline groundwater pumping

4.3.1. Aquifer salinity analysis

The position and shape of the FSI changes continuously during pumping in accordance with the measured EC profiles from the observation wells (Fig. 6). The FSI descends and is drawn toward the pumping wells (Fig. 6). There is a good correlation between the modeled and measured FSI depths in the three cross sections after 1 year (dashed lines, Fig. 6) and 12 years (solid lines, Fig. 6). The

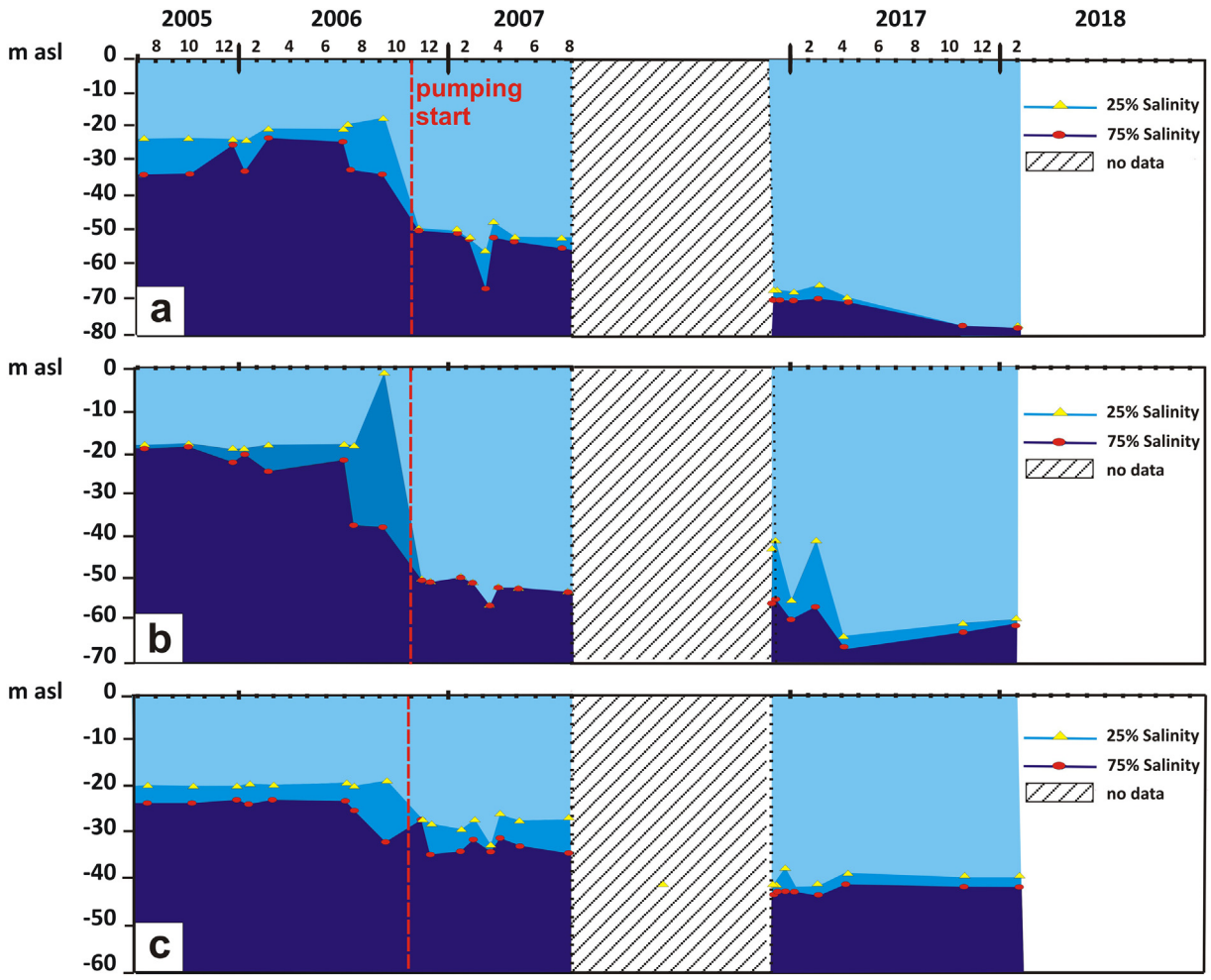

Fig. 4. Salinity evolution at boreholes P-I, P-II, and P-III (a, b, and c, respectively) over 12 years of pumping, as depicted from electrical conductivity (EC) measurements. The 25% and 75% EC lines were derived from seawater EC of 60 mS/cm. The light, intermediate, and dark blue zones represent freshwater, the interface zone, and saline water, respectively. The red vertical dotted lines represent pumping start. No data: period without data recording from September 2007 to October 2016.

greatest mismatch between the data and modeled FSI depth is in P-I after 1 year where the deviation is ~6 m. Most other deviations are less than 2 m (Fig. 6). This descent, resulting from SGW pumping, has previously been described both analytically (Otero et al., 2011) and numerically (Stein et al., 2019), by using sand tank experiments (Shi et al., 2011), and by using EC profiles from boreholes (Jorreto et al., 2009). However, all prior studies have been based solely on modeling or short-term field data.

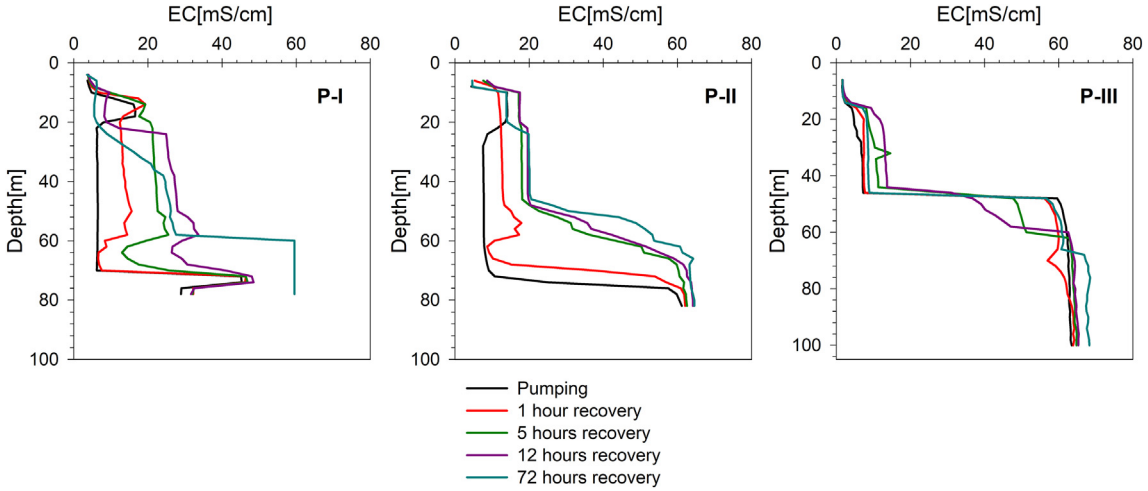

Fig. 5. Electrical conductivity (EC) profiles of P-I, P-II, and P-III observation boreholes during recovery at different times after pumping stop.

Table 2
Hydraulic parameters and boundary conditions used in the model after calibration.

Parameter	Unit	Value
Hydraulic conductivity [K]	m d^{-1}	65
Anisotropy of conductivity		0.2
Specific storage	m^{-1}	0.0001
Density ratio		0.025[a]
Porosity		0.15
Longitudinal dispersivity	m	7.5
Transverse dispersivity	m	0.25
Infiltration rate (Neumann BC)	mm yr^{-1}	30[b]
Horizontal inflow (Neumann BC)	mm d^{-1}	8.5

[a] Taken from (Ataie-Ashtiani et al., 1999).
[b] Taken from (Pulido-Bosch et al., 2012).

Despite the fact that all wells pump at the same rate, the zone surrounding P-I experiences the greatest FSI reduction. This can be explained by the higher density of pumping wells near P-I (Figs. 1,3), leading to a greater overall drawdown. The salinity distribution after 12 years of pumping is not uniform along the coast as can be seen in the cross sections shown in Fig. 7a(2–4) and in the 3D representation and map view in Fig. 8a and b respectively. The pumping wells' influence on the salinity distribution becomes progressively smaller with increasing distance from the center of the line of pumping wells (Fig. 7a2–4). Despite the fact that there is a pumping well next to P-III, its influence on the salinity distribution is lower than that of the pumping well next to P-I and P-II (Fig. 7a-2, 3).

To quantify the extent of freshening in the Andarax aquifer, the Φ ratio is calculated for the modeled aquifer in the domain of interest (DOI) that stretches below the land side of the aquifer according to Stein et al. (2019):

$$\Phi = \frac{M_t}{M_0} \quad (1)$$

where M_t is the modeled dissolved mass in the DOI (Fig. 3) after pumping, and M_0 is its value at steady state before pumping. Fig. 9a shows the progression of the Φ ratio over time for the Andarax aquifer. The ratio decreases as SGW is extracted (black solid line, Fig. 9), indicating aquifer freshening. The value of 0.84 after 12 years of pumping represents a 16% reduction in the salt content of the DOI. This salt content reduction accounts for the replacement of 2,560,000 m^3 of saline water with freshwater over the 12 years pumping period.

From this point, two potential scenarios are modeled: continuation of pumping for another 20 years at the same rate and cessation of pumping for 20 years with ensuing natural recovery of the aquifer to hydrostatic equilibrium. The first scenario is more likely to occur in reality, as the desalination plant is intended to continue to deliver potable water to Almeria. The second scenario predicts the rate of aquifer recovery if pumping were to stop. In the first case, the aquifer continues to freshen, albeit at a much lower rate, and reaches a Φ ratio of 0.83 after a total of 32 years of continuous pumping; that is, an additional 200,000 m^3 of freshwater replaces the saline water over the additional 20 years of pumping. In a similar 3D numerical model describing the coastal aquifer in Israel, Stein et al. (2019) showed that the aquifer reached $\Phi = 0.5$ after 20 years of pumping, lower than the $\Phi = 0.83$ after 20 years predicted here. Both studies described the DOI similarly and scenarios of identical pumping rate are compared. The difference can be attributed to the difference in hydraulic conductivity (35 m d^{-1}, compared with 65 m d^{-1} in the present study) and freshwater influx (200 mm yr^{-1} compared with 30 mm yr^{-1} in this study). The model sensitivity analysis reported by Stein et al. (2019) showed that a higher hydraulic conductivity of the aquifer correlates with a higher Φ ratio as a result of pumping SGW. Furthermore, it also emphasizes the importance of the fresh influx boundary condition, as higher influx results in lower Φ ratio.

In the second case, the long-term recovery scenario simulates the aquifer for 20 years following the cessation of pumping after 12 years. The FSI geometry dynamics modeled during recovery (Fig. 10) show the progression of the 50% salinity contour at P-I, as this well experienced the greatest changes. The FSI moves rapidly at first, as clearly observed after 1–3 days. After 5 years without pumping, the FSI shifts back to its original shape and location as it was before pumping. These results are consistent with the Φ ratio analysis (Fig. 9a), which shows the fast initial recovery becoming slower over time. The Φ ratio of the aquifer increases continuously after pumping ceases, and reaches 0.95 after 15 years of recovery. After 20 years of recovery, the aquifer reaches steady state again at $\Phi = 0.99$. This model scenario exemplifies the timescale of aquifer restoration after pumping SGW at high rates for several years.

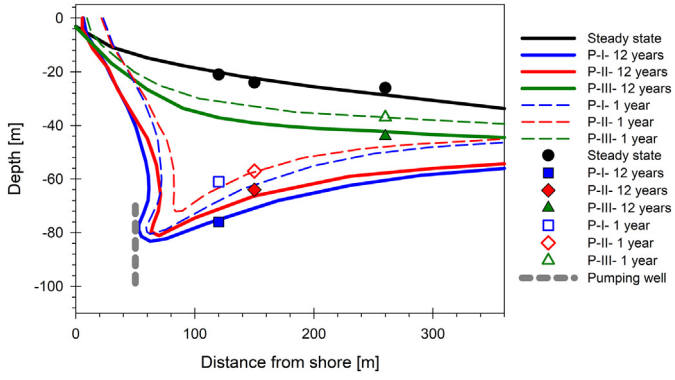

Fig. 6. Cross-sections (marked in Fig. 1) showing 50% salinity lines of the 3D model and measured data points. All symbols represent measurement points of the FSI location in the observation wells. The solid black line represents steady state, while the colored solid lines represent 50% salinity in the three cross sections after 12 years of pumping (P-I, blue; P-II, red; P-III, green) or after 1 year of pumping (the dashed colored lines). The vertical grey dashed line represents the screen position of the pumping wells.

4.3.2. Pumped water salinity

To analyze the salinity of the groundwater pumped from the aquifer, the salinity in the well is calculated with time. The freshwater content in the SGW well is calculated according to the following equation after (Stein et al., 2019):

$$FW_{content} = 1 - \frac{S_t}{S_{sea}} \quad (2)$$

where S_t is the salinity in the pumping wells at a given time and S_{sea} is the sea salinity (35 g L^{-1}). Fig. 9b shows the pumping wells' salinity with time. The SGW salinity pumped from the wells decreases as pumping progresses until reaching steady salinity of 32.7 g L^{-1} after 5 years of pumping. After this time, the salinity remains constant, even after an additional 20 years of pumping. This indicates that the salinity in the well has reached steady state; however, steady state has not necessarily been reached in the aquifer. As mentioned previously, the salinity of the pumped water reported from the desalination plant is around 33 g L^{-1} which is in good agreement with the model results. On the other hand, when pumping ceases, the salinity at the pumping wells rapidly recovers, and after only 6 months, the salinity in the wells is predicted to be 35 g L^{-1} (Fig. 9b). It is important to note that for a desalination facility, knowledge of the water salinity is crucial as it directly influences the osmotic pressure and consequentially the applied pressure necessary for the process (Stein et al., 2016).

The freshwater flow rate into the 19 pumping wells is calculated (as two end members) as a function of time (Fig. S3) according to the equation by (Stein et al., 2019):

$$Q_f = Q_t * FW_{content} \quad (3)$$

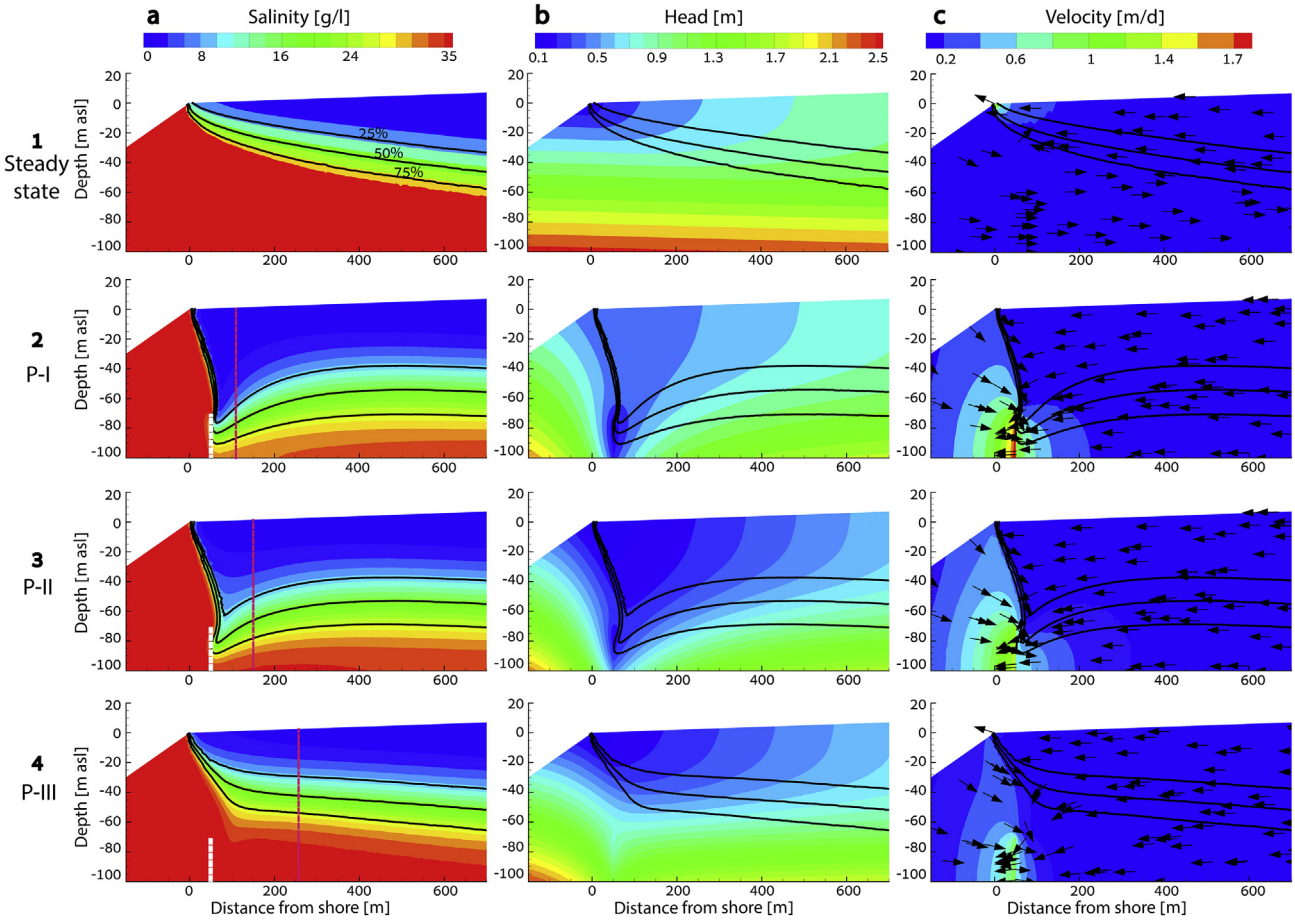

Fig. 7. Zoom-in on cross sections of (1) steady state, (2) P-I, (3) P-II and (4) P-III showing distribution of (a) salinity, (b) hydraulic head and (c) velocity vectors. These cross sections correspond to those depicted in Fig. 1, and represent the salinity profiles after 12 years of pumping. The three black lines in all panels represent the 25%, 50% and 75% salinity contour lines (as shown in panel 1a). Column a (rows 2–4) shows the pumping well location (vertical white dashed line) and the observation well locations (vertical purple dashed lines). These features are not shown in all panels due to masking of data in the panels.

where Q_f is the freshwater pumping rate and Q_t is the total pumping rate. The freshwater pumping rate increases as pumping continues until reaching a steady rate of 3190 $m^3\ d^{-1}$ after 5 years.

4.3.3. Hydraulic head and water velocity distribution

The pumping wells' radius of influence overlap, and superposition of the pumping creates a unique distribution of the hydraulic heads (Fig. 7b). Close to P-I (Fig. 7b-2), the lowest hydraulic head is where the pumping well is situated. Farther away along the line of pumping wells, closer to P-III (Fig. 7b-4), the hydraulic head distribution is different. The hydraulic head in this location tends to reach steady state where the lowest value is on the ocean floor close to the shore (Fig. 7b-1).

At steady state before pumping, the SGW flows inland (below the FSI) and the freshwater flows seaward (above the FSI) (Oz et al., 2015) (Fig. 7c-1). However, commencement of pumping SGW induces radial flow to the well. Some freshwater flows into the well instead of being discharged into the ocean, and SGW flow (below the FSI) changes its direction seaward into the well (Fig. 7c 2–4). Despite the fact that the pumping wells draw water radially, the water flow velocity is not

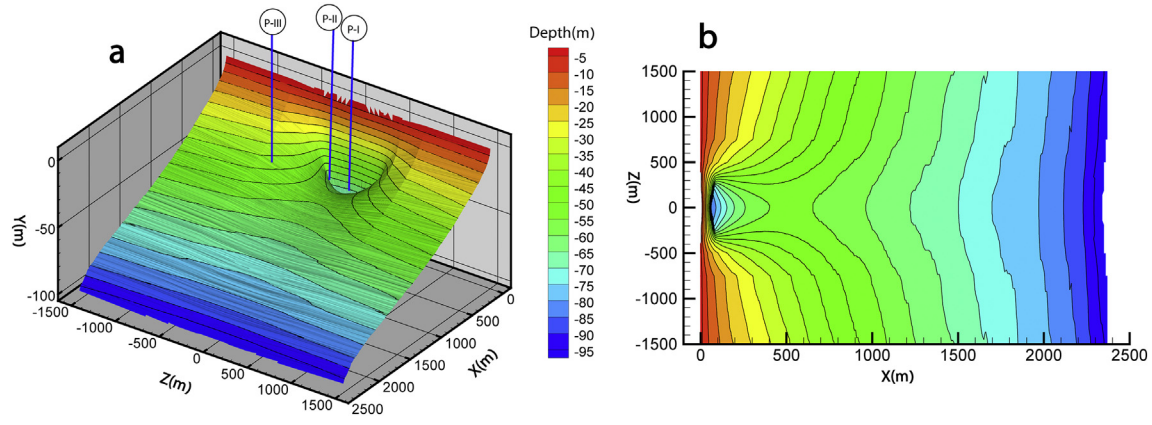

Fig. 8. Visualization of the modeled 50% salinity surface (i.e., the FSI) after 12 years of pumping (a) 3D, (b) map view. Colors represent the FSI depth below sea level.

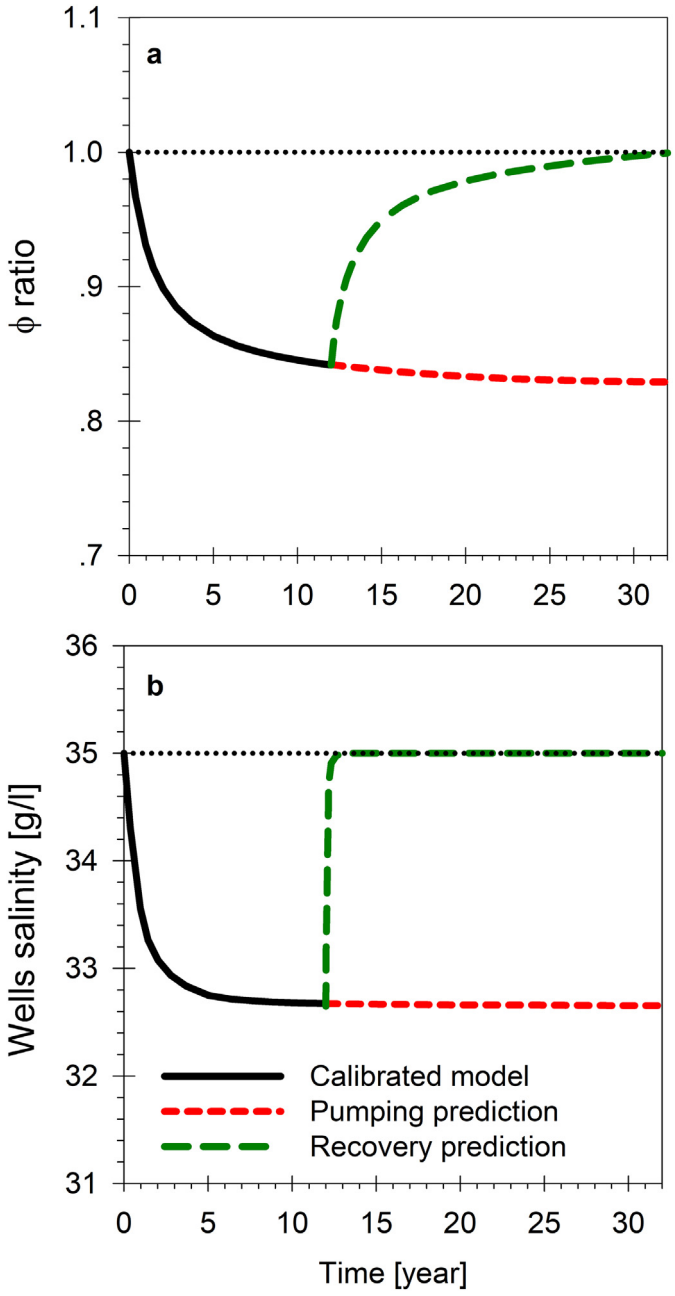

Fig. 9. The Φ ratios predicted using the calibrated model (black line), assuming pumping for another 20 years (red line), and the predicted recovery of the aquifer over the 20 years following a pumping stop (green line).

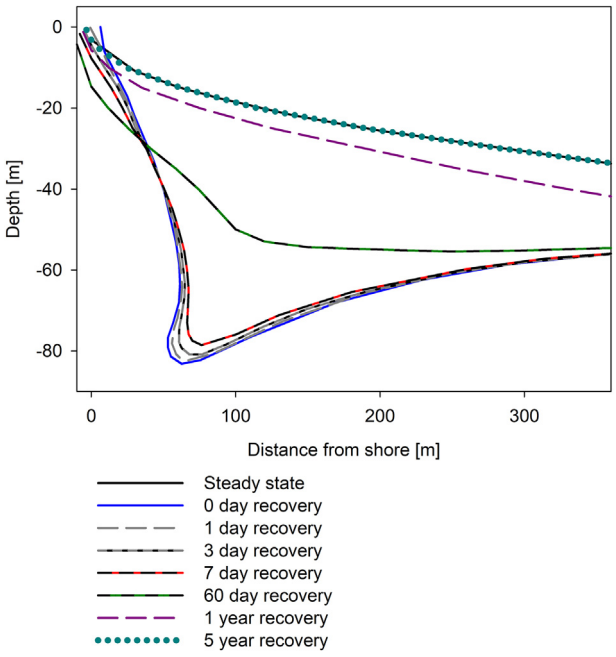

Fig. 10. Modeled 50% salinity contours of the long-term recovery at P-I; solid lines represent the initial (pumping) and final (steady-state) cases, and dashed lines represent the interface at different times during recovery.

distributed evenly around the wells. Pumping of SGW results in higher velocity vectors from the sea side than from the land side (Fig. 7c 2–4). This is due to the complex dynamics of fresh and saline water in the coastal zone. On the landward side, the flux is limited due to lack of rain and constant flux (constant Neumann boundary condition), while on the seaside, the pumping wells are closer to the prescribed head sea boundary condition that allows for the compensation of the abstraction of the pumping wells. This can happen only under the condition that there is a clear connection between the aquifer and the sea. In addition, in the absence of pumping, the natural flow of SGW is landward. When pumping begins, SGW on the landward side of the well reverses its direction, flowing toward the pumping well at a rate that is proportional to the head gradient in the pumping period minus the natural flow head gradient. The velocity of the SGW on the sea side of the pumping well is increased, as the velocity from pumping is added to the natural gradient. Therefore, most of the saline water that flows to the wells comes from the seaside rather than the land side (Fig. 7c).

4.3.4. Drawdown analysis

The drawdown pattern of the area above the pumping well near P-I (which experienced the highest drawdown) is plotted in Fig. 11a. The model shows that within 50 days of pumping start, the drawdown reaches a maximum of 0.53 m. As pumping progresses, the drawdown decreases and reaches a steady value of 0.22 m after two years. As previously noted, the FSI shifts downward toward the well immediately after pumping start, resulting in replacement of SGW with freshwater from above. This phenomenon can be explained due to the fact that the rate of the FSI movement (~0.25 m d^{-1}) is greater than that of freshwater from recharge (~0.05 m d^{-1}) which eventually fills the cone of depression until the water table reaches a new steady state. Pumping for an additional 20 years does not change the drawdown any further (Fig. 11a) due to the fact that relatively small amounts of freshwater flow to the well and the fresh natural flow is able to compensate for the freshwater loss to pumping.

As pumping ceases, the drawdown pattern above the pumping wells changes rapidly (Fig. 11a). At first, the water table rises to 0.22 m above its natural steady-state location. Following the rapid rise of the water table, it slowly returns to its natural water level. This occurs due to the rapid upward FSI movement, which pushes the freshwater above it upward, creating a water table mound above the pumping wells. As recovery of the aquifer continues, the upward FSI movement slows, while the excess freshwater is discharged to the sea. This phenomenon can be observed in the submarine groundwater discharge (SGD) flux rate (Fig. 11b). The SGD flux pattern is a mirror image of the drawdown pattern. After pumping stops, the SGD rate rapidly increases above its natural rate before slowly returning to its natural rate. The fast movement of the FSI upward "squeezes" the freshwater body above, increasing the water table height, which in turn increases the gradient seaward. This occurs due to higher velocity of the FSI upward than the freshwater seaward. The height of the freshwater layer is decreased while the discharge remains the same. Ultimately, this results in a temporary increase in SGD velocity.

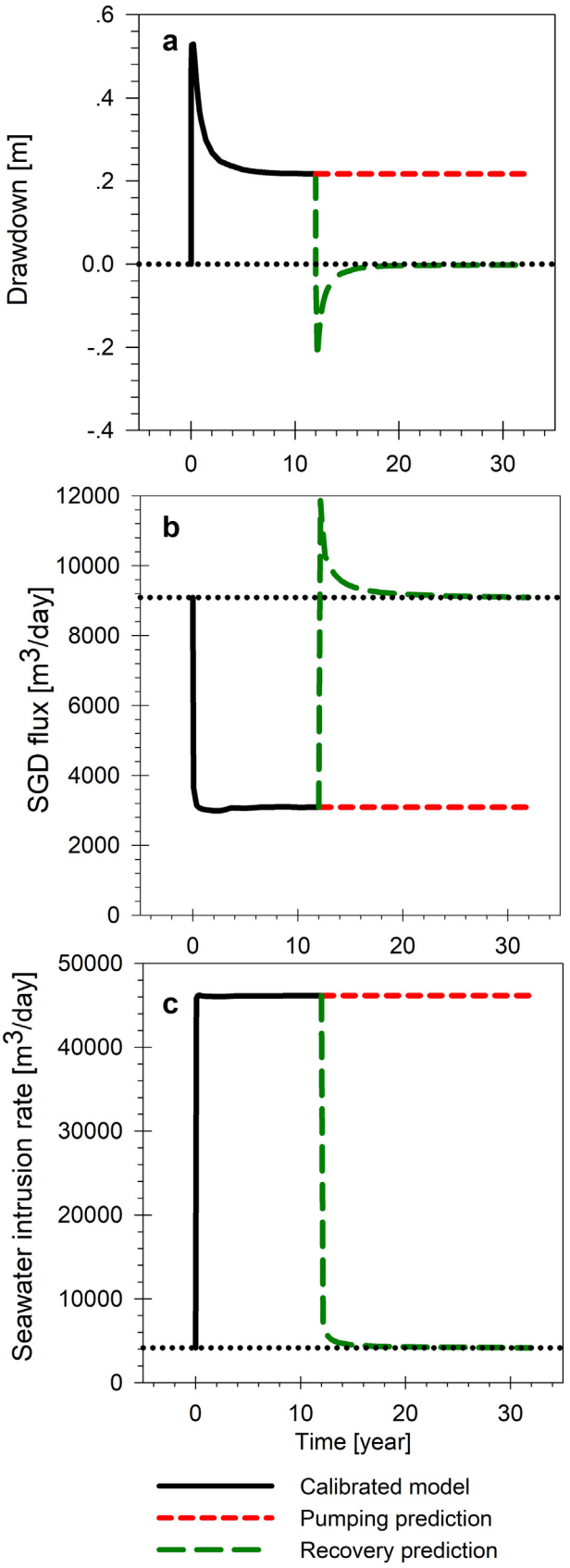

Table 3
SGD components (fresh and saline groundwater) at steady state before pumping start and after 12 years of pumping.

Time [year]	Total SGD [m^3 d^{-1}]	Fresh SGD [m^3 d^{-1}]	Saline SGD [m^3 d^{-1}]	Fresh to saline ratio
0	9090	4900	4160	1.19
12	3090	1750	1350	1.30

4.3.5. Water budget analysis

The volume of freshwater recharge from precipitation and inflow in the model is calculated to be ~4900 m^3 d^{-1}. At steady state without pumping, this is the same rate as freshwater discharge to the sea. Saline water is also discharged at a rate equal to the natural seawater intrusion rate (Burnett et al., 2006; Wilson, 2005). However, within a few days of the pumping start, the total (fresh and saline) SGD drops significantly from ~9090 m^3 d^{-1} to ~3090 m^3 d^{-1}, which then remains steady (Fig. 11b). The SGD flux decreases after pumping start, as the freshwater flux vectors above the pumping wells are diverted toward the wells.

Shortly after pumping start, the seawater intrusion rate increases from a steady state of ~4160 m^3 d^{-1} to a new steady state of ~46,000 m^3 d^{-1} (Fig. 11c). It is important to note that the pumping rate of 4000 m^3 h^{-1} is applied only for 12 h a day, yielding a daily pumping rate of 48,000 m^3 d^{-1}. Therefore, most of the intruded seawater is ultimately extracted from the pumping wells and does not travel further inland. The rest of the water pumped from the wells is a combination of saline and fresh water from the land side.

After pumping ceases, the seawater intrusion rate immediately drops, reaching a rate of 5550 m^3 d^{-1} after 6 months and then slowly decreases to a steady state rate of ~4160 m^3 d^{-1} after 20 years of recovery. The reason the seawater intrusion rate does not reach steady state immediately after pumping cessation is that the aquifer is not at a steady hydraulic head and salinity distribution, and saline water is required to replace freshwater in order to reach hydrostatic equilibrium. Only when hydrostatic equilibrium is achieved, the natural seawater intrusion rate returns to its natural magnitude.

The new steady state of fresh SGD rate is calculated using the following equation:

$$SGD_{FW} = Reacharge\ rate + inflow\ rate - Q_f \quad (4)$$

Saline SGD rate is evaluated by the total SGD minus SGD_{FW}. This equation is true only after a new steady state has been reached. Analysis of the modeled SGD components (fresh and saline) reveals that most of the SGD is composed of freshwater. This analysis is in line with an extensive numerical study that was conducted in North Carolina (Wilson, 2005) and with SGD field measurements from the shore of Japan (Taniguchi et al., 2006). These studies showed that close to shore, the majority of SGD is freshwater rather than saline. Table 3 shows the components of the SGD before pumping and after 12 years of pumping.

The fresh to saline SGD ratios show that after a new steady state is reached, more freshwater is discharged to the sea than saline water. This indicates that saline water accounts for most of the water flowing into the well from the land-side. The model results show that the volume of freshwater that has not been lost to the sea due to pumping of SGW for 12 years is 19,300,000 m^3. Furthermore, the reduction of the

Fig. 11. (a) The drawdown above the pumping well at the P-I cross section, (b) the volumetric SGD flux and (c) the seawater intrusion rate predicted by the calibrated model (black line), assuming pumping for another 20 years (red line), and the predicted recovery of the aquifer over the 20 years following a stop to pumping (green line). Black dotted lines represent the steady state. The drawdown is calculated as the initial water table height above sea level before pumping minus water table height at a given time. Negative values indicate that the water table is higher than it was before pumping start.

Table 4
Sensitivity analysis of aquifer recovery. Simulation 0 indicates the calibrated model parameters. Bolded font represents the hydraulic parameters and normal font represent the resulting parameters.

Simulation	Hydraulic conductivity [m d^{-1}]	Porosity	Specific storage [m^{-1}]	Anisotropy of conductivity	FW inflow [mm d^{-1}]	Dispersivity [m] [a]	Φ ratio	% Deviation	SGD flux [m^3 d^{-1}]	% deviation of SGD flux	SW intrusion rate [m^3 d^{-1}]	% deviation of SW intrusion rate
0	**65**	**0.15**	**0.0001**	**0.2**	**8.58**	**7.5**	1.00	0	9098	0	4161	0
1	**75**	**0.15**	**0.0001**	**0.2**	**8.58**	**7.5**	1.05	5.2	9861	8.4	4924	18.3
2	**55**	**0.15**	**0.0001**	**0.2**	**8.58**	**7.5**	0.94	5.8	8320	8.5	3383	18.7
3	**65**	**0.075**	**0.0001**	**0.2**	**8.58**	**7.5**	1.02	1.6	9051	0.5	4114	1.1
4	**65**	**0.3**	**0.0001**	**0.2**	**8.58**	**7.5**	0.98	1.7	9163	0.7	4225	1.5
5	**65**	**0.15**	**0.00001**	**0.2**	**8.58**	**7.5**	1.00	0.2	9100	0.02	4163	0.05
6	**65**	**0.15**	**0.001**	**0.2**	**8.58**	**7.5**	1.00	0.3	9086	0.13	4149	0.3
7	**65**	**0.15**	**0.0001**	**0.3**	**8.58**	**7.5**	1.00	0.4	9262	1.8	4325	3.9
8	**65**	**0.15**	**0.0001**	**0.1**	**8.58**	**7.5**	0.99	0.9	8261	9.2	3323	20.1
9	**65**	**0.15**	**0.0001**	**0.2**	**4.33**	**7.5**	1.14	13.8	7608	16.4	4524	8.7
10	**65**	**0.15**	**0.0001**	**0.2**	**17.08**	**7.5**	0.76	24.3	12,243	34.6	3600	13.5
11	**65**	**0.15**	**0.0001**	**0.2**	**8.5**	**5**	1.01	0.8	8493	6.6	3556	14.5
12	**65**	**0.15**	**0.0001**	**0.2**	**8.5**	**15**	0.97	2.8	9906	8.9	4969	19.4

[a] The longitudinal to transverse dispersivity ratio was kept 30 like in the calibrated model.

discharge of freshwater to the sea stabilizes after 6 years of pumping at ~1,100,000 m^3 yr^{-1}.

4.4. Sensitivity analysis

Sensitivity analysis was performed to identify the factors affecting the recovery of the aquifer. Different hydraulic parameters were changed in each scenario, and the model was run for 20 years with no pumping. Table 4 gives the results. The most influential hydraulic parameter in aquifer recovery on the salinity distribution (Φ ratio) was the freshwater inflow, defined by the total freshwater inflow to the model (recharge + inflow). The hydraulic conductivity was the second most influential parameter. These two parameters were also the most influential on the SGD flux in aquifer recovery. However, the most influential parameter on the seawater intrusion rate was the hydraulic conductivity and the hydraulic conductivity anisotropy. These parameters have previously been shown to be the most influential on seawater intrusion in natural conditions, during freshwater pumping (Filippis et al., 2016; Zeng et al., 2018) and during SGW pumping from the coastal aquifer (Stein et al., 2019). Another influential parameter on the seawater intrusion rate is the dispersivity of the aquifer that is as influential to the model results as the hydraulic conductivity.

5. Summary and conclusions

Intensive pumping of saline groundwater from the Almeria coastal aquifer has pushed the FSI toward the pumping wells, freshening significant parts of the coastal aquifer (observed in three observation wells). Long-term monitoring revealed that the FSI descended by up to 20 m within the first year of pumping, and it continued to drop to 50 m after 12 years of pumping. Short-term interface monitoring after the cessation of pumping revealed a rapid upward movement of the interface, suggesting that the aquifer was returning to its natural steady state location.

A 3D finite element model of the aquifer was designed, implemented, and calibrated with the long-term EC measurements taken at the three observation wells. The uneven distribution of pumping wells and superposition of the pumping influence resulted in a "salinity sink" in the interface within the area of higher pumping-well density. The model predicted that continuous pumping for an additional 20 years would not significantly change the salinity of the aquifer near the pumping wells. Furthermore, if pumping were to stop, the aquifer would return to a steady state, and the FSI would shift upward toward its original hydrostatic equilibrium. The recovery rate was highest immediately after the pumping stopped, and the interface developed its original shape after several months. However, the aquifer did not fully return to its original location ($\Phi = 0.99$) until only 20 years of no pumping had passed.

The model further demonstrated that pumping saline water from below the FSI would push the interface downward quickly at first, creating higher-than-normal drawdown of the fresh groundwater above. Freshwater flow would then fill the cone of depression until the drawdown reaches a new steady state. As a result of SGW pumping, the SGD rate is predicted to decrease significantly due to freshwater flow to the vicinity of the pumping wells. In addition, seawater intrusion rate would increase tenfold following the pumping start; however, most of the water would be extracted by the pumping wells. Most saline water flowing to the pumping wells comes from seawater intrusion from the sea side rather than the land side. These findings are important for coastal aquifer management and planning wells for pumping SGW to a desalination plant. Furthermore, this work describes an additional advantage of using SGW for desalination, as pumping saline water from below the FSI creates a barrier to seawater intrusion.

CRediT authorship contribution statement

Shaked Stein: Methodology, Validation, Formal analysis, Investigation, Resources, Data curation, Writing - original draft, Visualization. **Fernando Sola:** Conceptualization, Methodology, Validation, Formal analysis, Investigation, Data curation, Writing - original draft, Visualization. **Yoseph Yechieli:** Conceptualization, Writing - review & editing, Supervision, Resources, Project administration. **Eyal Shalev:** Conceptualization, Resources, Writing - review & editing, Visualization, Supervision. **Orit Sivan:** Writing - review & editing, Supervision, Resources, Project administration. **Roni Kasher:** Writing - review & editing, Supervision, Resources. **Angela Vallejos:** Conceptualization, Methodology, Validation, Resources, Writing - original draft, Visualization, Supervision, Project administration, Funding acquisition.

Declaration of competing interest

The authors declare that they have no known competing financial interests or personal relationships that could have appeared to influence the work reported in this paper.

Acknowledgments

This work is part of the general research lines promoted by the CEIMAR Campus of International Excellence, and it was supported by MINECO and FEDER through Project CGL2015-67273-R. We thank the Israeli Water Authority for the scholarship to SS and the Rieger Foundation-JNF for their generous support. Support was also provided to SS by the Mediterranean Sea Research Center of Israel.

Appendix A. Supplementary data

Supplementary data to this article can be found online at https://doi.org/10.1016/j.scitotenv.2020.139249.

References

Aguirre, J., Braga, J.C., Jiménez, A.P., Rivas, P., 1996. Substrate-related changes in pectinid fossil assemblages. Palaeogeogr. Palaeoclimatol. Palaeoecol. 126 (3–4), 291–308. https://doi.org/10.1016/S0031-0182(96)00042-9.

Ataie-Ashtiani, B., Volker, R.E., Lockingtonb, D.A., 1999. Tidal effects on sea water intrusion in unconfined aquifers. J. Hydrol. 216 (216), 17–31.

Bear, J., 1972. Dynamics of Fluids in Porous Media. Elsevier, New York.

Bear, J., 1979. Hydraulics of Groundwater. McGraw-Hill Publishing Company.

Burnett, W.C., Aggarwal, P.K., Aureli, A., Bokuniewicz, H., Cable, J.E., Charette, M.A., et al., 2006. Quantifying submarine groundwater discharge in the coastal zone via multiple methods. Sci. Total Environ. 367 (2–3), 498–543. https://doi.org/10.1016/j.scitotenv.2006.05.009.

Cooper, H.H., 1959. A hypothesis concerning the dynamic balance of fresh water and salt water in a coastal aquifer. J. Geophys. Res. 64 (4), 461–467. https://doi.org/10.1029/jz064i004p00461.

Custodio, E., Bruggeman, G.A., 1987. Studies and Reports in Hydrology: Groundwater Problems in Coastal Areas in. UNESCO, Paris.

Daniele, L., Vallejos, A., Sola, F., Corbella, M., Pulido-Bosch, A., 2011. Hydrogeochemical processes in the vicinity of a desalination plant (Cabo de Gata, SE Spain). Desalination 277 (1–3), 338–347. https://doi.org/10.1016/j.desal.2011.04.052.

Dehwah, A.H.A., Missimer, T.M., 2016. Subsurface intake systems: green choice for improving feed water quality at SWRO desalination plants, Jeddah, Saudi Arabia. Water Res. 88, 216–224. https://doi.org/10.1016/j.watres.2015.10.011.

Dhar, A., Datta, B., 2009. Saltwater intrusion management of coastal aquifers. I: linked simulation-optimization. J. Hydrol. Eng. 14 (12), 1263–1272. https://doi.org/10.1061/(asce)he.1943-5584.0000097.

Diersch, H.J.G., Kolditz, O., 2002. Variable-density flow and transport in porous media; approaches and challenges. *25 Years*. Adv. Water Resour. 25 (8–12), 899–944. https://doi.org/10.1016/S0309-1708(02)00063-5.

Ferguson, G., Gleeson, T., 2012. Vulnerability of coastal aquifers to groundwater use and climate change. Nat. Clim. Chang. 2 (5), 342–345. https://doi.org/10.1038/nclimate1413.

Filippis, G. De, Giudici, M., Margiotta, S., 2016. Conceptualization and characterization of a coastal multi-layered aquifer system in the Taranto gulf (southern Italy). Environ. Earth Sci. 75 (8), 1–17. https://doi.org/10.1007/s12665-016-5507-7.

Ghaffour, N., Missimer, T.M., Amy, G.L., 2013. Technical review and evaluation of the economics of water desalination: current and future challenges for better water supply sustainability. Desalination 309, 197–207. https://doi.org/10.1016/j.desal.2012.10.015 2013.

Ghaffour, N., Bundschuh, J., Mahmoudi, H., Goosen, M.F.A., 2015. Renewable energy-driven desalination technologies: a comprehensive review on challenges and potential applications of integrated systems. Desalination 356, 94–114. https://doi.org/10.1016/j.desal.2014.10.024.

Houben, G., Post, V.E.A., 2017. The first field-based descriptions of pumping-induced saltwater intrusion and upconing. Hydrogeol. J. 25 (1), 243–247. https://doi.org/10.1007/s10040-016-1476-x.

Jakovovic, D., Werner, A.D., de Louw, P.G.B., Post, V.E.A., Morgan, L.K., 2016. Saltwater upconing zone of influence. Adv. Water Resour. 94, 75–86. https://doi.org/10.1016/j.advwatres.2016.05.003.

Jorreto, S., Pulido-Bosch, A., Gisbert, J., Sánchez-Martos, F., Francés, I., 2009. The fresh water-seawater contact in coastal aquifers supporting intensive pumped seawater extractions: a case study. Comptes Rendus - Geoscience 341 (12), 993–1002. https://doi.org/10.1016/j.crte.2009.08.001.

Kazakis, N., Spiliotis, M., Voudouris, K., Pliakas, F.K., Papadopoulos, B., 2018. A fuzzy multicriteria categorization of the GALDIT method to assess seawater intrusion vulnerability of coastal aquifers. Sci. Total Environ. 621, 524–534. https://doi.org/10.1016/j.scitotenv.2017.11.235.

Knight, A.C., Werner, A.D., Morgan, L.K., 2018. The onshore influence of offshore fresh groundwater. J. Hydrol. 561, 724–736. https://doi.org/10.1016/j.jhydrol.2018.03.028.

Kohout, F.A., 1960. Cyclic flow of salt water in the Biscayne aquifer of southeastern Florida. J. Geophys. Res. 65 (7), 2133–2141. https://doi.org/10.1029/jz065i007p02133.

Levanon, E., Yechieli, Y., Shalev, E., Friedman, V., Gvirtzman, H., 2013. Reliable monitoring of the transition zone between fresh and saline waters in coastal aquifers. Groundwater Monitoring and Remediation 33 (3), 101–110. https://doi.org/10.1111/gwmr.12020.

Levanon, E., Yechieli, Y., Gvirtzman, H., Shalev, E., 2017. Tide-induced fluctuations of salinity and groundwater level in unconfined aquifers – field measurements and numerical model. J. Hydrol. 551, 665–675. https://doi.org/10.1016/j.jhydrol.2016.12.045.

Loáiciga, H.A., Pingel, T.J., Garcia, E.S., 2012. Sea water intrusion by sea-level rise: scenarios for the 21st century. Ground Water 50 (1), 37–47. https://doi.org/10.1111/j.1745-6584.2011.00800.x.

Michael, H.A., Mulligan, A.E., Harvey, C.F., 2005. Seasonal oscillations in water exchange between aquifers and the coastal ocean. Nature 436 (7054), 1145–1148. https://doi.org/10.1038/nature03935.

Missimer, T.M., Ghaffour, N., Dehwah, A.H.A., Rachman, R., Maliva, R.G., Amy, G., 2013. Subsurface intakes for seawater reverse osmosis facilities: capacity limitation, water quality improvement, and economics. Desalination 322, 37–51. https://doi.org/10.1016/j.desal.2013.04.021.

Nocchi, M., Salleolini, M., 2013. A 3D density-dependent model for assessment and optimization of water management policy in a coastal carbonate aquifer exploited for water supply and fish farming. J. Hydrol. 492, 200–218. https://doi.org/10.1016/j.jhydrol.2013.03.048.

Otero, N., Soler, A., Corp, R.M., Mas-Pla, J., Garcia-Solsona, E., Masqué, P., 2011. Origin and evolution of groundwater collected by a desalination plant (Tordera, Spain): a multi-isotopic approach. J. Hydrol. 397 (1–2), 37–46. https://doi.org/10.1016/j.jhydrol.2010.11.020.

Oz, I., Shalev, E., Yechieli, Y., Gvirtzman, H., 2015. Saltwater circulation patterns within the freshwater-saltwater interface in coastal aquifers: laboratory experiments and numerical modeling. J. Hydrol. 530, 734–741. https://doi.org/10.1016/j.jhydrol.2015.10.033.

Pool, M., Carrera, J., 2009. Dynamics of negative hydraulic barriers to prevent seawater intrusion. Hydrogeol. J. 18 (1), 95–105. https://doi.org/10.1007/s10040-009-0516-1.

Pulido-Bosch, A., Delgado, J., Sola, F., Vallejos, Á., Vicente, F., López-Sánchez, J.M., Mallorquí, J.J., 2012. Identification of potential subsidence related to pumping in the Almería basin (SE Spain). Hydrol. Process. 26 (5), 731–740. https://doi.org/10.1002/hyp.8181.

Pulido-Bosch, A., Vallejos, A., Sola, F., 2019. Methods to supply seawater to desalination plants along the Spanish mediterranean coast and their associated issues. Environ. Earth Sci. (322), 78 https://doi.org/10.1007/s12665-019-8298-9.

Rachman, R.M., Li, S., Missimer, T.M., 2014. SWRO feed water quality improvement using subsurface intakes in Oman, Spain, Turks and Caicos Islands, and Saudi Arabia. Desalination 351, 88–100. https://doi.org/10.1016/j.desal.2014.07.032.

Rau, G.C., Post, V.E.A., Shanafield, M., Krekeler, T., Banks, E.W., Blum, P., 2019. Error in hydraulic head and gradient time-series measurements: a quantitative appraisal. Hydrol. Earth Syst. Sci. 23 (9), 3603–3629. https://doi.org/10.5194/hess-23-3603-2019.

Rodríguez-Estrella, T., Pulido-Bosch, A., 2009. Methodologies for abstraction from coastal aquifers for supplying desalination plants in the south-east of Spain. Desalination 249 (3), 1088–1098. https://doi.org/10.1016/j.desal.2009.06.046.

Ros, S.E.M., Zuurbier, K.G., 2017. The impact of integrated aquifer storage and recovery and brackish water reverse osmosis (ASRRO) on a coastal groundwater system. Water (Switzerland) 9 (4). https://doi.org/10.3390/w9040273.

Sanchez-Martos, F., Pulido-Bosch, A., Molina-Sanchez, L., Vallejos-Izquierdo, A., 2002. Identification of the origin of salinization in groundwater using minor ions (lower Andarax, Southeast Spain). Sci. Total Environ. 297, 45–58. https://doi.org/10.1016/S0048-9697(01)01011-7.

Sánchez-Martos, F., Jorreto, S., Gisbert, J., Vallejos, Á., Sola, F., Daniele, L., et al., 2007. Consideraciones hidrogeológicas sobre el control de la intrusión marina y la captación de agua de mar para desaladoras en Almería (SE España). Recorrido hidrogeológico por las desaladoras almerienses. Los acuíferos costeros: retos y soluciones, pp. 131–159 Almeria, Spain.

Shalev, E., Lazar, A., Wollman, S., Kington, S., Yechieli, Y., Gvirtzman, H., 2009. Biased monitoring of fresh water-salt water mixing zone in coastal aquifers. Ground Water 47 (1), 49–56. https://doi.org/10.1111/j.1745-6584.2008.00502.x.

Shi, L., Cui, L., Park, N., Huyakorn, P.S., 2011. Applicability of a sharp-interface model for estimating steady-state salinity at pumping wells-validation against sand tank experiments. J. Contam. Hydrol. 124 (1–4), 35–42. https://doi.org/10.1016/j.jconhyd.2011.01.005.

Sola, F., Vallejos, A., López-Geta, J.A., Pulido-Bosch, A., 2013. The role of aquifer media in improving the quality of seawater feed to desalination plants. Water Resour. Manag. 27 (5), 1377–1392. https://doi.org/10.1007/s11269-012-0243-6.

Sola, F., Vallejos, A., Daniele, L., Pulido-Bosch, A., 2014. Identification of a Holocene aquifer – lagoon system using hydrogeochemical data. Quat. Res. 82, 121–131.

Sreekanth, J., Datta, B., 2011. Optimal combined operation of production and barrier wells for the control of saltwater intrusion in coastal groundwater well fields. Desalin. Water Treat. 32 (1–3), 72–78. https://doi.org/10.5004/dwt.2011.2680.

Stein, S., Russak, A., Sivan, O., Yechieli, Y., Rahav, E., Oren, Y., Kasher, R., 2016. Saline groundwater from coastal aquifers as a source for desalination. Environ. Sci. Technol. 50 (4). https://doi.org/10.1021/acs.est.5b03634.

Stein, S., Yechieli, Y., Shalev, E., Kasher, R., Sivan, O., 2019. The effect of pumping saline groundwater for desalination on the fresh–saline water interface dynamics. Water Res., 46–57 https://doi.org/10.1016/j.watres.2019.03.003.

Strack, O.D.L., 1976. A single-potential solution for regional Interface problems in coastal aquifers. Water Resource Research 12 (6), 1165–1174.

Taniguchi, M., Ishitobi, T., Shimada, J., 2006. Dynamics of submarine groundwater discharge and freshwater-seawater interface. Journal of Geophysical Research: Oceans 111 (1), 1–9. https://doi.org/10.1029/2005JC002924.

Todd, D.K., Mays, L.W., 1980. *Groundwater Hydrology* (Third). Wiley.

Van Dam, J.C., 1999. Exploitation, restoration and management. Seawater Intrusion in Coastal Aquifers: Concepts, Methods and Practices. Kluwer Acad, Norwell, Mass, pp. 73–125.

Wang, J., Tsay, T.K., 2001. Tidel effects on groundwater motions. Transp. Porous Media 43 (1), 159–178. https://doi.org/10.1023/A:1010634114160.

Werner, A.D., Simmons, C.T., 2009. Impact of sea-level rise on sea water intrusion in coastal aquifers. Ground Water 47 (2), 197–204. https://doi.org/10.1111/j.1745-6584.2008.00535.x.

Werner, A.D., Jakovovic, D., Simmons, C.T., 2009. Experimental observations of saltwater up-coning. J. Hydrol. 373 (1–2), 230–241. https://doi.org/10.1016/j.jhydrol.2009.05.004.

Werner, A.D., Ward, J.D., Morgan, L.K., Simmons, C.T., Robinson, N.I., Teubner, M.D., 2012. Vulnerability indicators of sea water intrusion. Ground Water 50 (1), 48–58. https://doi.org/10.1111/j.1745-6584.2011.00817.x.

Werner, A.D., Bakker, M., Post, V.E.A., Vandenbohede, A., Lu, C., Ataie-Ashtiani, B., et al., 2013. Seawater intrusion processes, investigation and management: recent advances

and future challenges. Adv. Water Resour. 51, 3–26. https://doi.org/10.1016/j.advwatres.2012.03.004.
Wilson, A.M., 2005. Fresh and saline groundwater discharge to the ocean : a regional perspective. Water Resource Research 41, 1–11. https://doi.org/10.1029/2004WR003399.
Yechieli, Y., Shalev, E., Wollman, S., Kiro, Y., Kafri, U., 2010. Response of the Mediterranean and Dead Sea coastal aquifers to sea level variations. Water Resour. Res. 46 (12), 1–11. https://doi.org/10.1029/2009WR008708.
Yu, X., Michael, H.A., 2019. Offshore pumping impacts onshore groundwater resources and land subsidence. Geophys. Res. Lett. 46 (5), 2553–2562. https://doi.org/10.1029/2019GL081910.
Zeng, X., Dong, J., Wang, D., Wu, J., Zhu, X., Xu, S., et al., 2018. Identifying key factors of the seawater intrusion model of Dagu river basin , Jiaozhou Bay. Environ. Res. 165, 425–430. https://doi.org/10.1016/j.envres.2017.10.039 (August 2017).
Zhou, Q., Bear, J., Bensabat, J., 2005. Saltwater upconing and decay beneath a well pumping above an interface zone. Transp. Porous Media 61 (3), 337–363. https://doi.org/10.1007/s11242-005-0261-4.